Liquefaction of alpine lake sediments: predictive simulations and post-event validation at Spitallamm Reservoir

Carlo Rabaiotti[1*,2], *Pavel* Trapper[3], and *Reto* Schnellmann[4]
[1] Terraqua Engineering AG, Zollikerberg, Switzerland
[2] OST – Eastern Switzerland University of Applied Sciences, Rapperswil, Switzerland
[3] Ben-Gurion University of the Negev, Be'er Sheva, Israel
[4] Schläpfer & Partner AG, Zürich, Switzerland

Abstract. Fine-grained lacustrine sediments in alpine reservoirs may exhibit pronounced undrained instability when subjected to rapid hydraulic unloading. In this paper, static liquefaction denotes a monotonic, non-seismic undrained instability in which excess pore-pressure generation causes the mean effective stress to collapse towards zero, followed by rapid post-peak strength loss and flow-like deformation. Such stress paths can occur during reservoir drawdown or sudden depressurization of a buried hydraulic opening, even though fully drained dewatering would increase effective stress. This paper presents a documented case history from the Spitallamm reservoir (Switzerland), where the emptying of a disused tunnel inlet beneath the former lakebed triggered a collapse of saturated silty sediments. Prior to the operation - and before any direct geotechnical characterisation of the sediments was available - numerical simulations using PLAXIS (small strain, NorSand model) and ABAQUS (large strain, CEL) were conducted based on grain-size classification and literature parameters. The models predicted progressive loss of effective stress and failure by static liquefaction. Post-event CPTu, Ball-cone, and laboratory tests on undisturbed samples confirmed pronounced post-peak softening and liquefaction behaviour, validating the pre-event predictions. The results confirm that failure was governed by stress-path-dependent undrained instability rather than low peak strength, highlighting limitations of strength-based assessment for contractive lacustrine soft soils.

1 Introduction

Soft soils are commonly characterised by high water content, low permeability, and a mechanical response that is strongly governed by stress path, drainage conditions, and soil state. Lacustrine sediments fall within this category when deposited under low-energy conditions, forming fine-grained, weakly structured soils that may exhibit contractive behaviour and pronounced strain softening under undrained loading. In alpine reservoirs, such sediments accumulate over decades from glacial and proglacial inputs and are frequently subjected to variations in hydraulic boundary conditions associated with reservoir operation.

The susceptibility of saturated silts and fine sands to static liquefaction has been documented in both natural and engineered environments, including lacustrine basins, submarine slopes, and tailings facilities [1,2]. In the present paper, static liquefaction is defined as a monotonic undrained instability of a contractive saturated soil, in which the imposed stress path generates excess pore pressure, the mean effective stress approaches a near-zero state, and the soil loses shear resistance after peak strength. This definition distinguishes the mechanism considered here from drained dewatering: under fully drained conditions, lowering pore-water pressure would increase effective stress, whereas the observed collapse involved rapid unloading and local depressurization under essentially undrained conditions. These studies emphasise that instability is not controlled solely by peak shear strength, but by the soil state relative to the critical state, fabric, and fines content. For soft soils subjected to rapid unloading, undrained conditions may prevail, leading to excess pore-pressure generation, loss of effective stress, and post-peak strength degradation [3,4].

Alpine lacustrine sediments present additional complexity due to their layered structure, variable consolidation history, and occasional weak cementation. Field investigations indicate that such deposits may exhibit moderate to high undrained shear strength in penetration tests, while still remaining susceptible to stress-path–dependent instability [5,6]. This apparent contradiction highlights the limitations of strength-based characterisation alone when assessing soft soils prone to contractive behaviour.

From a soft-soil engineering perspective, these characteristics necessitate the use of constitutive models capable of reproducing undrained instability and post-peak softening. This paper addresses these issues through the analysis of lacustrine sediments exposed during reservoir drawdown at the Grimselsee, providing insight into the behaviour of soft alpine sediments under rapid unloading and the implications for their assessment and modelling in engineering practice.

Before reservoir drawdown, the available geotechnical information was limited to historical sedimentological observations, grain-size distributions, and general knowledge of comparable alpine lacustrine

* Corresponding author: carlo.rabaiotti@ost.ch

deposits. The numerical analyses presented in this paper were therefore first carried out as a predictive engineering assessment before tunnel emptying, using literature-based constitutive assumptions constrained by the observed depositional setting and slope geometry. After the drawdown and the collapse event, CPTu, Ball-cone, and laboratory testing on undisturbed samples became available. These post-event data are used here as an independent validation dataset and, where appropriate, to refine the interpretation of the mechanisms identified in the pre-event simulations.

2 Lake sediments at Spitallamm reservoir

2.1 Depositional setting

The lake sediments at Spitallamm are in the alpine reservoir of the Grimselsee upstream of the historic Spitallamm Dam. The reservoir occupies a glacially overdeepened basin underlain by stiff glacial and proglacial deposits. Since reservoir impoundment, fine-grained sediments have accumulated on the lakebed from suspended loads supplied by glacial meltwater and tributaries.

Deposition occurred predominantly under low-energy hydraulic conditions, leading to laminated silts and fine sands with seasonal variability. Repeated reservoir drawdown and refilling cycles induced alternating phases of deposition and reconsolidation, resulting in a stratified sediment body with variable density and consolidation state, characteristic of alpine lacustrine soft soils. Because such lacustrine deposits are typically normally consolidated to lightly overconsolidated and loose in their recently deposited upper layers, they are prone to contractive behaviour and may be susceptible to static liquefaction when rapid undrained unloading is imposed.

2.2 Preliminary mechanical characterisation

Prior to reservoir drawdown, geotechnical information on the sediments was limited. The preliminary stability assessment therefore relied on geomorphological observations, historical investigations, and analogy with comparable alpine lake deposits.

The sediments were interpreted as saturated, low-permeability soft soils, prone to undrained loading during rapid unloading events such as tunnel emptying. Based on observed depositional slopes near the tunnel inlet, the effective friction angle was conservatively estimated at approximately 25° [7].

Undrained shear strength was assumed to be moderate but strongly stress-path dependent, with a high susceptibility to pore-pressure build-up and post-peak softening under undrained conditions. These assumptions formed the basis of the initial numerical stability analyses.

2.3 Grain-size distribution and mineralogical composition

Post-drawdown investigations provided direct confirmation of sediment composition. Grain-size analyses indicate that the deposits are dominated by silt-sized particles with subordinate fine sand fractions and only minor clay content. Fines contents typically range from approximately 35% to 70%, and the sediments are predominantly classified as ML, SM, or SP–SM according to USCS [8]. The grain-size curves are narrow and poorly graded, consistent with suspension settling in calm lacustrine conditions. (Fig. 1).

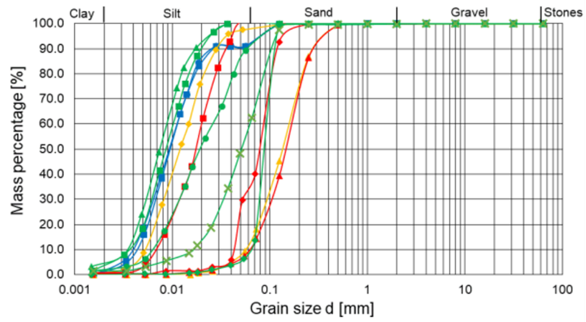

Fig. 1. Grain-size distribution of Spitallamm sediments.

Mineralogical analyses reported in the characterisation study [6] identify quartz and feldspar as the dominant phases, with significant contributions from mica and a non-negligible chlorite content. The presence of chlorite is interpreted as a potential source of weak interparticle bonding, leading to apparent cementation at small strains while not preventing contractive behaviour and strength loss at larger strains. (Fig. 2)

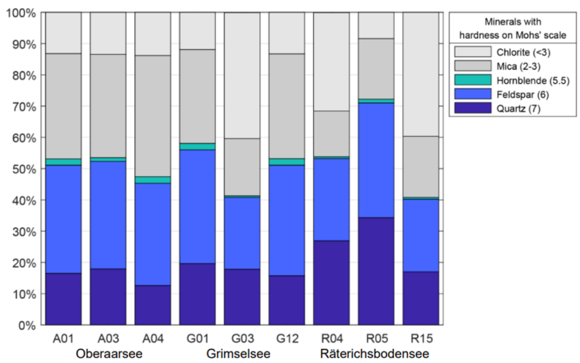

Fig. 2. Mineralogical composition of lacustrine sediments (after [6]).

3 Numerical modelling

3.1 Modelling strategy

Numerical analyses were carried out in two stages to address different parts of the problem. First, finite-element analyses in PLAXIS were used to study the pre-failure response of the sediments during rapid tunnel depressurization. The aim of this stage was to capture stress redistribution, excess pore-pressure generation, and the onset and spatial extent of undrained instability. Second, large-deformation analyses in ABAQUS/CEL were used to simulate post-failure motion of the liquefied sediments into the tunnel, a stage that cannot be represented reliably with conventional small-strain finite elements once large distortions develop.

This distinction is important because the paper documents a predictive analysis performed before the event and then evaluated against post-event observations. The PLAXIS simulations were part of the original engineering assessment undertaken before tunnel emptying. The field and laboratory investigations became available only after drawdown and are therefore used here to validate the predicted failure mechanism and to refine the constitutive interpretation.

3.2 Constitutive modelling

Field observations and post-event laboratory tests indicate that the Spitallamm sediments behave as contractive silty soils under undrained loading, with rapid pore-pressure build-up and marked post-peak strength loss. Such behaviour cannot be reproduced adequately with constitutive models that rely only on peak strength. For the pre-failure stage, a constitutive description is required that links shear deformation, volumetric tendency, effective stress change, and soil state relative to the critical state.

For this reason, the NorSand model was adopted in the PLAXIS analyses. NorSand is a critical state based elastoplastic model that can reproduce contractive and dilative response, strain softening, and static liquefaction. In the present study, grain-size distribution was used only to classify the sediments and to place them within plausible literature ranges for silty lacustrine soils. The pre-event parameter set was then selected from published ranges, depositional interpretation, observed slope geometry, and sensitivity analyses. After the event, undisturbed sampling and triaxial testing provided a basis for partial calibration of the parameters governing contractive response and post-peak softening. The manuscript therefore distinguishes between the assumed pre-event parameter set used for prediction and the post-event calibrated range used for interpretation.

For the large-deformation ABAQUS/CEL analyses, the objective was different. Once liquefaction is triggered, the key requirement is to simulate rapid strength loss, large strains, and sediment mobility in the tunnel geometry without mesh distortion. A simplified undrained strain-softening model with peak and residual shear strength was therefore adopted. This formulation does not aim to provide a full critical-state description; instead, it represents the post-trigger reduction in shear resistance that governs runout. The ABAQUS model should thus be interpreted as a post-failure mobility model that is informed by the mechanisms identified in PLAXIS and supported by the post-event laboratory evidence.

For comparison, additional PLAXIS analyses were performed using Mohr–Coulomb and hardening soil formulations. While these models provided reasonable estimates of initial stability, they were unable to reproduce progressive strength degradation or the liquefaction trigger, confirming the necessity of a critical-state-capable model for the pre-failure stage.

3.3 PLAXIS analyses

PLAXIS analyses were performed in two and three dimensions (Fig. 3). Initial conditions corresponded to fully saturated sediments under hydrostatic pore pressure. Tunnel emptying was simulated as rapid depressurisation under undrained conditions.

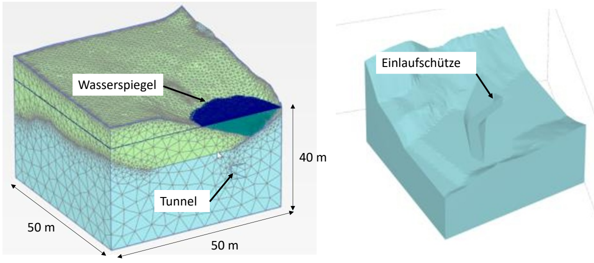

Fig. 3. PLAXIS model geometry and mesh (Wasserspiegel = water table; Einlaufschütze = tunnel inlet).

The results (Fig. 4 and Fig. 5) show excess pore-pressure induced liquefaction and localised plastic strains in silt-dominated layers. Instability initiates near the tunnel inlet and propagates upward, consistent with static liquefaction controlled by stress path rather than peak strength.

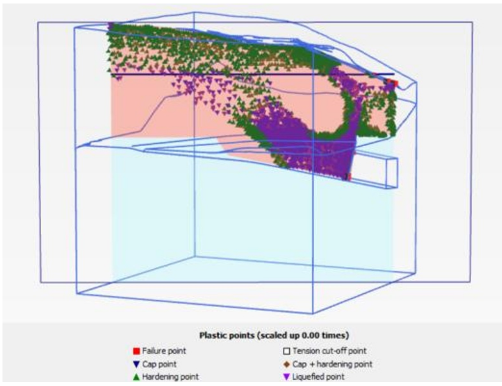

Fig. 4. PLAXIS simulation showing plastic points; liquefied points are shown in violet.

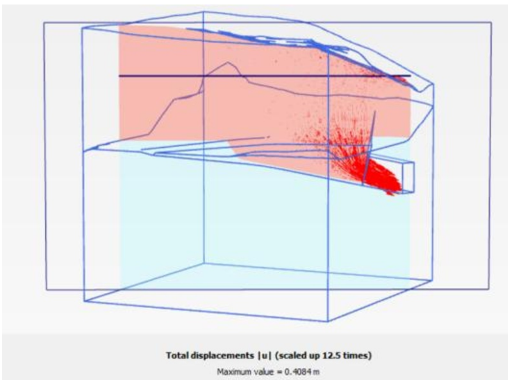

Fig. 5. PLAXIS simulation showing total displacement and plastic-strain localization near the tunnel inlet.

3.4 ABAQUS analyses

The large-deformation analyses were performed using the ABAQUS Coupled Eulerian–Lagrangian (CEL) formulation to simulate the post-failure evolution of the lacustrine sediments following depressurization. In this framework, the sediments and pore water were modelled as Eulerian materials, while rigid components such as bedrock, tunnel lining, and structural elements were represented as Lagrangian bodies. The CEL approach avoids excessive mesh distortion and allows realistic simulation of flow-like deformation after instability onset.

The model geometry and mesh are shown in Fig. 6. Sediments were modelled as a strain-softening Eulerian material; pore water was represented by an Eulerian formulation with a Mie-Grüneisen equation of state [14], while the tunnel and surrounding rock were treated as rigid Lagrangian bodies.

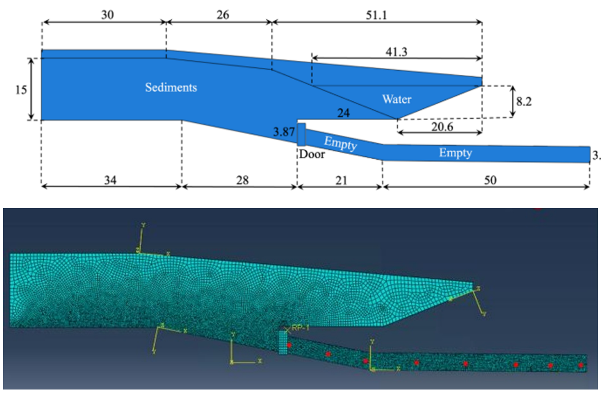

Fig. 6. ABAQUS model dimensions and CEL mesh. Red = location of the point for velocity assessment.

The simulations show rapid sediment acceleration once liquefaction is triggered, followed by sustained flow toward the tunnel (Fig. 7, Fig. 8). Several scenarios accounting for different residual strength and soil-tunnel friction were carried out. All scenarios indicate significant post-failure mobility.

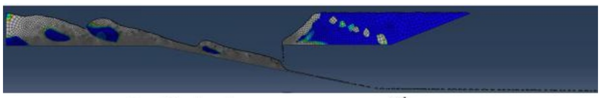

(a) Frictionless: $\tau_r = 10$ KPa , $\gamma_r^{pl} = 0.4$

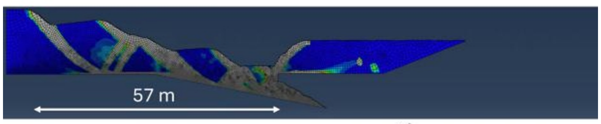

(b) Frictionless: $\tau_r = 30$ KPa , $\gamma_r^{pl} = 0.4$

Fig. 7. ABAQUS/CEL simulation showing the extent of the failure zone for frictionless contact between sediment and tunnel inlet under two residual shear strengths: (a) 10 kPa and (b) 30 kPa.

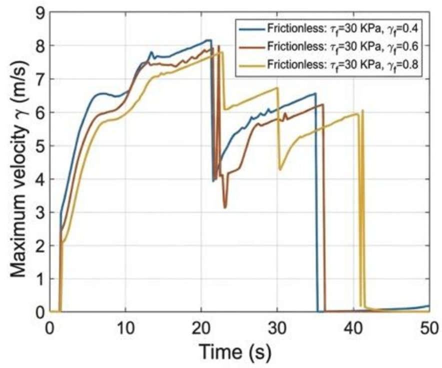

(a)

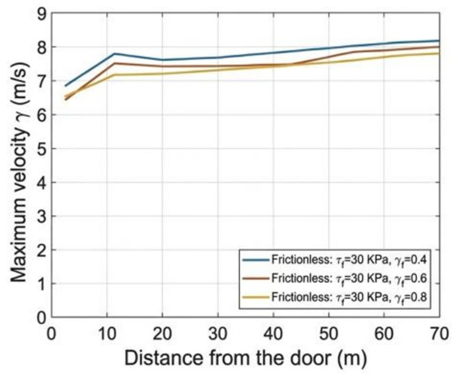

(b)

Fig. 8. Sediment velocity in the tunnel for three residual-strength scenarios: (a) maximum velocity versus time and (b) maximum velocity versus distance from the tunnel inlet.

4 Laboratory testing

Undisturbed samples recovered from the sediments were tested under undrained triaxial conditions representative of rapid unloading [8]. The tests reveal pronounced contractive behaviour with rapid pore-pressure accumulation after peak deviatoric stress. In several cases, effective stress reduces to near zero, indicating static liquefaction.

Calibration (Fig. 9 and Fig. 10) of synthetic experiments carried out with the soil test in PLAXIS and the constitutive model NorSand (parameters given in Table 1) reproduced the experimental results well, despite challenges in specimen preparation for undisturbed silty samples.

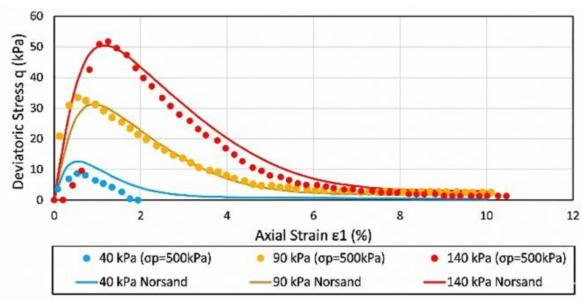

Fig. 9. Undrained stress-strain response.

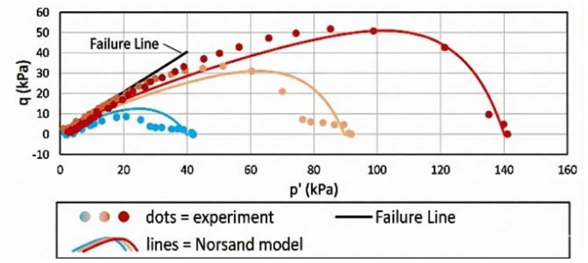

Fig. 10. Effective stress paths. The initial discrepancy for the probes at lower confining pressures (yellow and blue) is attributed to slight loading asymmetry arising from the challenging preparation of undisturbed silty specimens.

Table 1. NorSand parameters used in the study.†

Parameter	Unit	[8]	[7]	[10]
G_{ref}	kN/m²	4000 – 7000	2000	4000 – 8000
P_{ref}	kN/m²	100	100	100
n_G	–	0.2	0.45	0.4 – 0.7
ν	–	0.3	0.3	0.2 – 0.3
Γ	–	1.50	1.04	0.9 – 1.4
λ_e	–	0.01-0.03	0.024	0.01 – 0.07
M_{tc}	–	1.0 – 1.25	1.00	1.20 – 1.40
N	–	0.38	0.38	0.20 – 0.50
χ_{tc}	–	12 - 14	7.3	2.5 – 4.5
H_0	–	156	156	50 – 300
H_ψ	–	756	756	500 – 1000
R	–	1.0	1.0	≈ 1.0
S	–	1.0	1.0	0.8 – 1.2
Φ_0	–	0.04 / −0.005	0.03	0.02 – 0.06

† Table 1 *combines literature ranges, the pre-event parameter set adopted in the original engineering assessment, and the post-event calibrated range from triaxial testing. It should not be interpreted as implying that NorSand parameters can be derived from grain-size distribution alone. Grain-size data only constrain the soil type and plausible parameter bounds. Final parameter selection requires constitutive judgement and, where available, calibration against element tests. In particular, the calibrated values of* χ_{tc} *are higher than those commonly reported for many sandy soils and should be interpreted as material-specific fitting parameters required to reproduce the strongly contractive response of the tested silty lacustrine samples rather than as generic values for such sediments.*

The laboratory results demonstrate stress-path–dependent instability and explain the observed failure despite moderate peak strength.

5 In-situ testing

Post-event CPTu and Ball-cone testing was carried out after reservoir drawdown to characterize the sediment stratigraphy and to estimate mobilized undrained resistance. The results show a layered deposit with moderate to locally high penetration resistance, but also a consistently positive pore-pressure response in the fine-grained intervals, indicating contractive behaviour under undrained loading.

The most critical interval lies between approximately 2.1 m and 4.8 m depth. In this zone, CPTu indicates undrained shear strengths on the order of about 46.5 to 61.6 kPa, whereas laboratory triaxial tests on undisturbed samples yield lower values of about 20 to 28 kPa once post-peak softening is considered. Ball-cone cycling in the upper fine-grained sequence additionally showed pore-pressure accumulation and transient stiffness loss, consistent with a liquefaction-prone response. At greater depths, both CPTu and Ball-cone indicate progressively higher resistance and a transition to denser, more stable sediments.

These data help explain why the sediments could fail despite apparently moderate to high in-situ strength. Penetration tests mainly reflect peak or mobilized resistance during monotonic loading and are valuable for stratigraphic interpretation and for identifying contractive layers through their pore-pressure response. They do not, however, capture the post-peak softening and residual resistance that govern static liquefaction and flow failure. The discrepancy between CPTu/Ball-cone strengths and laboratory triaxial results in the 2.1 to 4.8 m interval therefore supports the interpretation that failure was controlled by stress-path-dependent instability rather than by low peak strength alone.

Table 2. Comparison of undrained shear strength, from laboratory (Triax) and field (CPTu, BC) tests.*

Depth[m]	(S_u) Triax [kPa]	(S_u) CPTu [kPa]	(S_u) BC [kPa]
0.0–0.6	-	0 – 52.6	35–45
0.6–2.1	27 - 45	32.0–41.3	30–40
2.1–4.8	20 - 28	46.5–61.6	-
4.8–6.0	25 - 65	95.7–134.9	-
6.0–9.0	73 - 112	76.7–109	100–115

** Liquefaction-susceptible interval (see Section 5); note discrepancy between field and laboratory Su values*

The CPTu-derived undrained shear strength profiles from the three soundings (SB1, SB2, SB3) are shown in Fig. 11. The data reveal a marked increase in S_u with depth below approximately 4 m, with considerable variability across soundings, reflecting the heterogeneous and layered nature of the lacustrine deposit. In the upper 2 m, near-zero to low values indicate very soft, recently deposited material. Between 2.1 and 4.8 m — the critical depth range identified in the PLAXIS analyses — CPTu-derived strengths are moderate (approximately 46–62 kPa) but overestimate the post-peak resistance measured in undrained triaxial tests, consistent with contractive behaviour and liquefaction susceptibility in that interval.

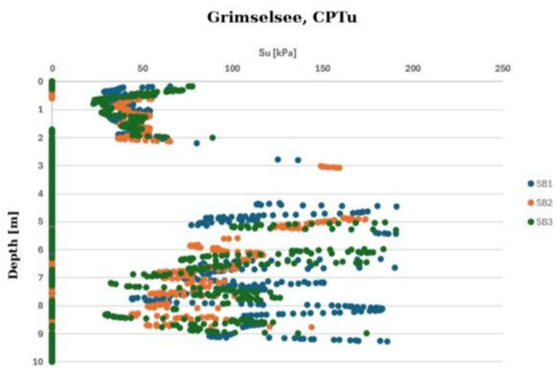

Fig. 11. CPTu-derived undrained shear strength S_u versus depth at Grimselsee, from three soundings (SB1, SB2, SB3). Positive pore-pressure response throughout the profile is consistent with contractive behaviour. The critical interval at 2.1-4.8 m depth shows lower S_u from laboratory triaxial tests (Table 2) compared to CPTu estimates, consistent with post-peak softening and static liquefaction susceptibility.

6 Collapse

The collapse occurred immediately after depressurization of the diversion tunnel, when hydrostatic support at the buried inlet was suddenly removed. Before depressurization, the saturated sediments in front of the inlet were laterally supported by the water pressure inside the tunnel. The rapid loss of this support imposed an undrained stress path on the surrounding silty sediments, promoting excess pore-pressure generation and a rapid reduction in effective stress.

Failure initiated at the tunnel entrance and propagated upward into the sediment body. The resulting geometry is steep and funnel-shaped, with near-vertical boundaries and no clear rotational slip surface. This morphology is more consistent with an internally triggered undrained instability than with a conventional shallow slope failure. Once the critical zone in front of the inlet lost effective stress, the sediment mass transitioned into a flow-like state and was drawn downward into the tunnel.

This interpretation is consistent with the modelling framework adopted in the paper. The PLAXIS analyses identify the location of instability initiation and the upward propagation of the failure zone from the inlet, while the ABAQUS/CEL analyses reproduce the subsequent large-deformation runout into the tunnel. The event should therefore be viewed as a two-stage process: initiation by static liquefaction under rapid unloading, followed by post-failure sediment mobility governed by residual undrained resistance and interface conditions inside the tunnel.

As illustrated in Fig. 12, the vertical red line marks the main collapse axis, corresponding to the zone of maximum stress concentration and sediment mobilisation. The short horizontal red marker identifies the approximate position of the tunnel inlet, where lateral support was removed during depressurization. From this location, sediments were drawn downward and inward, flowing directly into the tunnel.

The absence of a distinct rotational slip surface and the highly disturbed structure of the remaining sediment indicate that the failure mechanism was governed by static liquefaction. The collapse progressed rapidly and without observable precursory cracking or progressive deformation at the ground surface. The strong correspondence between the predicted failure path and the observed collapse geometry provides validation of the adopted modelling approach.

This event demonstrates that fine-grained lacustrine sediments can undergo sudden and severe instability when subjected to rapid depressurization, even when in-situ testing indicates moderate to high undrained shear strength. The collapse highlights the critical role of pore-pressure generation and post-peak strength degradation and confirms the necessity of explicitly considering liquefaction-type mechanisms in similar dam and reservoir engineering applications.

Fig.12. Collapse of lacustrine sediments following depressurization of the diversion tunnel. The vertical red line indicates the main collapse axis and direction of sediment displacement, while the dashed line indicates the approximate extent of the failed mass.

7 Conclusions

This paper documents a rare case of static liquefaction in fine-grained alpine lacustrine sediments triggered by rapid depressurization at a buried tunnel inlet. A key feature of the study is that the initial numerical analyses were performed before the event, using only limited pre-drawdown information, and were subsequently evaluated against post-event field and laboratory data.

The combined evidence shows that failure was governed by stress-path-dependent undrained instability rather than by low peak strength. CPTu and Ball-cone tests indicated moderate to locally high mobilized resistance, but laboratory triaxial tests on undisturbed samples revealed strong contractive response and pronounced post-peak softening in the critical depth range. The collapse mechanism observed in the field is therefore consistent with effective-stress collapse followed by flow-like sediment motion into the tunnel.

The hierarchical modelling approach proved effective. PLAXIS with a critical-state-based constitutive model captured the onset and geometry of the instability, whereas ABAQUS/CEL with a simplified strain-softening formulation was required to simulate post-failure mobility. The close correspondence between predicted failure location and observed collapse geometry provides confidence in the adopted framework.

From an engineering perspective, the case shows that fine-grained reservoir sediments may remain highly vulnerable to rapid unloading even when conventional in-situ strength indicators appear reassuring. Assessment of similar buried hydraulic structures should therefore consider contractive behaviour, excess pore-pressure generation, and post-peak strength loss explicitly, rather than relying on peak strength alone.

The authors gratefully acknowledge Kraftwerke Oberhasli AG (KWO) for their support and for granting access to the Spitallamm site and associated data. Special thanks are extended to Pascal Vollenweider, Andres Fankhauser, and Daniel Bürki for their valuable collaboration, technical input, and constructive discussions throughout the investigation and analysis phases. Their practical insight and continuous support were essential to the successful completion of this work.

References

1. A. Burghignoli, S. Miliziano, F.M. Soccodato, Cementation effects in two lacustrine clayey soils. Geotech. Geol. Eng. 28, 815–833 (2010) https://doi.org/10.1007/s10706-010-9343-3
2. B. Caicedo, C. Mendoza, A. Lizcano, F. Lopez-Caballero, Mechanical behaviour of lacustrine deposits. J. Rock Mech. Geotech. Eng. **11**, 837–849 (2019) https://doi.org/10.1016/j.jrmge.2018.12.016
3. P. Trapper, A. Puzrin, and L. Germanovich, Effects of shear band propagation on early waves generated by initial breakoff of tsunamigenic landslides. Mar. Geol. **370**, 99-112 (2015) https://doi.org/10.1016/j.margeo.2015.10.014
4. A. Stoecklin, P. Trapper, A. Puzrin, Controlling factors for post-failure evolution of subaqueous landslides. Géotechnique **71**, 879–892 (2020) https://doi.org/10.1680/jgeot.19.P.230
5. A. Lancini, Proglacial sedimentation in the Oberaar and Grimsel reservoirs. Diploma Thesis, ETH Zürich (2004)
6. A. Prohaska, D. Felix, Investigation on fine sediments in alpine reservoirs. VAW–ETH Zürich Report (2017)
7. C. Rabaiotti, P. Trapper, R. Schnellmann, Stability analysis of the Spitallamm tunnel inlet under reservoir drawdown. Terraqua Engineering AG Report, Switzerland (2024)
8. C. Rabaiotti, P. Trapper, R. Schnellmann, Geotechnical investigation of lacustrine sediments at Spitallamm. Terraqua Engineering AG / OST Report, Switzerland (2024)
9. M.G. Jefferies, NorSand: A simple critical state model for sand. Géotechnique **43**, 91–103 (1993) https://doi.org/10.1680/geot.1993.43.1.91
10. M.G. Jefferies, D.A. Shuttle, Dilatancy in generalised critical state models. Géotechnique **52**, 625–638 (2002) https://doi.org/10.1680/geot.2002.52.9.625
11. H. Liu, S. Nagula, H.P. Jostad, L. Piciullo, F. Nadim, Static liquefaction of tailings dams. Comput. Geotech. **167**, 106089 (2024) https://doi.org/10.1016/j.compgeo.2024.106089
12. A.M. Puzrin, E.E. Alonso, N. Pinyol, *Geomechanics of Failures*. Springer, New York (2010) https://doi.org/10.1007/978-90-481-3531-8
13. L.J. Woudstra, Verification and application of the NorSand model in PLAXIS. MSc Thesis, TU Delft (2021) https://resolver.tudelft.nl/uuid:dc29fd0a-6e8a-4f94-92d1-cd7b9a66c4fa
14. Dassault Systèmes, *ABAQUS Theory Manual*. Providence, RI (2023)